Proceedings of the Project Review, Geo-Mathematical Imaging Group (Purdue University, West Lafayette IN), Vol. 1 (2009) pp. 59-70.

DYNAMICALLY-FOCUSED GAUSSIAN BEAMS FOR SEISMIC IMAGING

ROBERT L. NOWACK*

Abstract. In this paper, an initial study is performed in which dynamically-focused Gaussian beams are investigated for seismic imaging. This work extends the work of Nowack (2008) in which the focusing Gaussian beams away from the source and receiver plane was implemented to allow the narrowest and planar portions of the beams to occur at the depth of a specific target structure. To match the seismic data, quadratic phase corrections are required for the local slant stacks of the data. To provide additional control of the imaging process, dynamic focusing is investigated where all sub-surface points are specified to have the same planar beam fronts. This gives the effect of using non-diffracting beams, but actually results from the use of multiple focusing depths for each beam. However, now different local slant stacks must be performed depending on the position of the sub-surface scattering point. To speed up the process, slant stacking of the local data windows is varied to match the focusing depths along individual beams when tracked back into the medium. The approach is tested with a simple model of 5 point scatterers which are then imaged with the data, and then to the imaging of a dynamically focused beam from the Sigsbee2A model.

1. Introduction. Dynamically-focused Gaussian beams are investigated for the seismic imaging of common-shot reflection data. This work extends the work of Nowack (2008) in which focusing of Gaussian beams away from the source and receiver surface is used to allow the narrowest portions of the beams to occur at the depth of a specific target structure. The beam fronts at the beam-waists are also planar leading to more stable beam summations for imaging. To match with the surface data, quadratic phase corrections are required for the local slant-stacks of the data. However, in the earlier approach only a single focusing depth can be specified. To provide additional control on the imaging process using focusing Gaussian beams, a dynamic process is investigated where all subsurface points are specified to have planar beams of the same width. This gives the effect of using non-diffracting beams, but actually results from the use of multiple imaging depths for each beam. As a result, there is a tradeoff in speed where now different slant stacks of the data are required for each subsurface point. In order to speed up the imaging process, the slant stacking of the data window is varied to match the focusing depths along individual beams when tracked back into the medium. These focused slant stacks are then matched to Gaussian beams with beam waists located at different sub-surface locations. The approach is first tested using 5 point scatterers which are then imaged with the data, and then using a dynamically-focused beam from the Sigsbee2A model.

Summations of Gaussian beams have been applied for the computation of high-frequency seismic wavefields in smoothly varying inhomogeneous media (see for example, Popov, 1982; Cerveny et al. 1982; Nowack and Aki, 1984). Reviews of Gaussian beam summation have been given by Cerveny (1985a,b), Babich and Popov (1989), and more recently by Popov (2002), Nowack (2003), Cerveny et al. (2007) and Bleistein (2007). An advantage of summations using Gaussian beams to construct more general wavefields is that the individual Gaussian beams have no singularities along their paths, no two-point ray tracing is required and triplicated arrivals are naturally incorporated into either forward or inverse modeling. More recently over-complete frame-based Gaussian beam summations have been developed based on window and wavelet transforms to address some of the issues related to completeness of beam summations (Lugara et al., 2003). In an over-complete frame based approach, the wavefield is decomposed into beam fields that are localized both in position and direction. Although an orthonormal basis cannot be formed using a Gabor frame, an over-complete frame expansion can be constructed which has the added benefit of providing redundancy in the expansion (Feichtinger and Strohmer, 1998; Hill; 1990, 2001; Hale, 1992, Nowack et al., 2003). Here curved initial beams are used to decompose the data and these are then propagated into the subsurface using dynamically-focused Gaussian beams.

In order to test the dynamically-focused Gaussian beam approach, a model is constructed with 5 small scatterers with depth in a vertically varying medium resulting in five diffracted arrivals each with different move-outs with distance. The partial image is then given for a single beam with different focusing depths such that the planar beam waists at the subsurface points are the same.

*Dept. of Earth and Atmos. Sci., Purdue University, West Lafayette, IN 47907, USA (nowack@purdue.edu).

However, when summed over all angles and data windows, the scatterers are properly imaged. This is then tested for a dynamically-focused beam from the Sigsbee2a model. The advantage of using dynamically-focused beams is the consistency of having the same focused beams for all sub-surface points. A disadvantage is that now multiple beam stacks are required for different points of the sub-surface which increases the computational burden compared to a standard Gaussian beam algorithm or a beam algorithm with a single focus depth. This can in part be offset by pre-computing the beam stacks at a set number of focusing depths and then interpolating the results required at different sub-surface points.

2. Gaussian Beam Imaging with Dynamically-Focused Beams. In common-shot migration, each shot gather is migrated separately and the results are summed to give the final image. Thus,

$$\delta m(\underline{x}) \sim \int d\underline{x}^s I^s(\underline{x}) \ , \tag{2.1}$$

where the adjoint image for each shot point can be written

$$I^s(\underline{x}) = \int \frac{d\omega}{2\pi} K(\omega) \int d\underline{x}^g \overline{g}(\underline{x}, \underline{x}^s, \omega) \overline{g}(\underline{x}, \underline{x}^g, \omega) u_s(\underline{x}^g, \underline{x}^s, \omega) \ , \tag{2.2}$$

and

$$K(\omega) = \omega^2 \bar{S}(\omega) \ . \tag{2.3}$$

From reciprocity of the Green's function $g(x, x^{'}, \omega) = g(x^{'}, x, \omega)$ and $\overline{g}$ indicates the complex conjugate of g.

In the 2-D case, the Green's function can be written in terms of a summation of Gaussian beams as

$$g(\underline{x}, \underline{x}', \omega) = \frac{-\mathrm{i}}{4\pi} \left(\frac{\varepsilon}{v_0} \right)^{1/2} \int d\gamma u_\gamma^{\mathrm{gb}}(\underline{x}, \underline{x}', \omega) = \frac{-\mathrm{i}}{4\pi} \left(\frac{\varepsilon}{v_0} \right)^{1/2} \int \frac{\mathrm{dp}_1^r}{p_3^r} u^{\mathrm{gb}}(\underline{x}, \underline{x}', \underline{p^r}, \omega) \tag{2.4}$$

where ε is the beam parameter (Cerveny et al., 1982), and

$$u_\gamma^{\mathrm{gb}}(\underline{x}, \underline{x}', \omega) = \left[\frac{v(s)}{q(s)} \right]^{1/2} \exp \left\{ \mathrm{i}\omega\tau(s) + \frac{\mathrm{i}\omega}{2} M(s) n^2 \right\} \tag{2.5}$$

The coordinates (*s*,*n*) correspond to the position $\underline{x}$ in ray centered coordinates, *τ(s)* is the travel-time along the central ray, *v(s)* is the velocity along the central ray and the horizontal component of the ray parameter vector at the source is $p_1^r = \sin\gamma / v_0$.

The complex second derivative of the travel-time field with respect to the transverse coordinate n can be written

$$M(s) = M_R(s) + \mathrm{i} M_I(s) = p(s)/q(s) \tag{2.6}$$

where $M_R(s)$ is related to the wavefront curvature $K(s)$ of the beam by $M_R(s) = K(s)/v(s)$. To form a bounded beam, then $M_I(s) > 0$. The variables $p(s)$ and $q(s)$ are solutions to the dynamic ray equations and for a beam solution are also complex (Cerveny, 2000). The dynamic ray equations in 2D have two real fundamental solutions which can be written as

$$\pi(s, s_0) = \begin{bmatrix} q_1(s) & q_2(s) \\ p_1(s) & p_2(s) \end{bmatrix} \tag{2.7}$$

where $\pi(s_0, s_0) = I$. $q_1(s)$, and $p_1(s)$ are solutions for an initial plane wave and $q_2(s)$ and $p_2(s)$ are for an initial point source. The inverse of $\pi(s, s_0)$ is

$$\pi^{-1}(s, s_0) = \pi(s_0, s) = \begin{bmatrix} p_2(s) & -q_2(s) \\ -p_1(s) & q_1(s) \end{bmatrix} \tag{2.8}$$

The two real solutions of the dynamic ray equations must then be combined to form a beam. There are a number of ways to combine the solutions, but one way is (Cerveny et al., 1982)

$$q(s) = \varepsilon q_1(s) + q_2(s) \tag{2.9}$$

and

$$p(s) = \varepsilon p_1(s) + p_2(s) \tag{2.10}$$

where ε is the beam parameter. The variable $q(s)$ is related to the complex geometrical spreading along the beam. Since for the fundamental solution matrix $Det(\pi(s, s_0)) = 1$ for all points along the ray, the complex geometric spreading can never be zero at any point along the beam if it is non-zero at any one point. Since the beam amplitude is related to the inverse square root of the geometric spreading, the beam amplitudes are always finite, even at caustics for the ray solution. This is one of the useful features of beam solutions, in contrast to ray solutions.

The second derivative of the time field with respect to n can be written as

$$M(s) = M_R(s) + \mathrm{i}M_I(s) = \frac{\varepsilon p_1(s) + p_2(s)}{\varepsilon q_1(s) + q_2(s)} \tag{2.11}$$

Since at the source point $\pi(s_0, s_0) = I$ and $\varepsilon = \varepsilon_R - \mathrm{i}\varepsilon_I$, then

$$M(s_0) = M_R(s_0) + \mathrm{i}M_I(s_0) = \frac{1}{\varepsilon} = \frac{\varepsilon_R}{\varepsilon^*\varepsilon} + \frac{\mathrm{i}\varepsilon_I}{\varepsilon^*\varepsilon} \tag{2.12}$$

where $\varepsilon^*\varepsilon$ is the magnitude squared of ε. Alternatively, ε can be written in terms of $M(s_0)$ as

$$\varepsilon = \frac{M_R(s_0)}{M^*(s_0)M(s_0)} - \frac{\mathrm{i}M_I(s_0)}{M^*(s_0)M(s_0)} \tag{2.13}$$

where $M^*(s_0)M(s_0)$ is the magnitude squared of $M(s_0)$. Thus, the complex beam parameter can be specified either directly in terms of ε or in terms of $M(s_0)$.

The complex beam parameter can also be written

$$\varepsilon = \varepsilon_r - \mathrm{i}\varepsilon_i = v_0 S_0 - \mathrm{i}v_0 L_0^2 \tag{2.14}$$

where v_0 is an initial velocity. In a homogeneous medium, S_0 is the distance of the beam waist from the initial point of beam.

An alternate, and in some sense simpler way, to blend the solutions to the dynamic ray equations is

$$q(s) = q_1(s) + M(s_0)q_2(s) \tag{2.15}$$

and

$$p(s) = p_1(s) + M(s_0)p_2(s) \tag{2.16}$$

where $M(s) = M_R(s) + \mathrm{i}M_I(s) = 1/\varepsilon$.

In either case, we can can obtain $M(s)$ at the scattering point, from the initial value of $M(s_0)$ along the source and receiver array by solving the dynamic ray equations for $p(s)$ and $q(s)$ and then forming $M(s) = p(s)/q(s)$. Alternatively, we can specify $M(s)$ at the scattering point, which I will denote as $M^e(s)$ for the ending point at the scatterer and then use the solution matrix for the dynamic ray equation $\pi(s_0, s)$ from s to s_0 to obtain $p(s_0)$ and $q(s_0)$ at the initial point of the ray. From these, one can obtain the corresponding value of beam curvature $M^b(s_0)$ at the beginning point of the ray. At a point along the beam, $M(s)$ can be written

$$M(s) = M_R(s) + \mathrm{i}M_I(s) = K(s)/v(s) + \mathrm{i}M_I(s) \tag{2.17}$$

where $K(s)$ is the wavefront curvature in ray coordinates and $v(s)$ is the velocity along the ray, and $M_I(s)$ is related to the transverse beam width. This can be specified at the endpoint of the ray and then be used to determine the value at the beginning point of the ray.

The exponential term away from the central ray can be written

$$\exp\left\{\frac{-\omega}{2}M_I(s)n^2\right\} = \exp\left\{\frac{-n^2}{2L^2(s)}\right\} \tag{2.18}$$

where $L(s) = (\omega M_I(s))^{-1/2}$ is the beam half-width transverse to the ray. At the initial point of the beam, $L(s_0) = (\omega M_I(s_0))^{-1/2} = (\frac{\varepsilon^* \varepsilon}{\omega \varepsilon_I})^{1/2}$. For the case of the beam waist at the initial point of the beam $M_R(s_0) = 0$, and $L(s_0) = (\frac{v_0}{\omega})^{1/2} L_0$ is the beam half-width at the beam-waist. In a homogeneous medium, this is the narrowest point along the beam and is also the only point where the beam front is planar. For the case when $M_R(s) = 0$ where $s \neq s_0$, the beam front is planar at some point s along the ray and generally curved at the initial position $s = s_0$. Also, the beam-waist is shifted along the beam away from the initial point of the beam.

Although the planar beam-waist is often placed at the initial source point for forward modeling, it is also common to put the beam-waist at the receiver location (Cerveny, 1985a,b). This reduces the number of beams required for the summation at the receiver, and also planar beam fronts at the receiver provide more stable beam summations. Recent true amplitude migration formulations using Gaussian beams have used beams launched directly from the scattering points up to the surface with the beam-waists specified at the scattering points (Protasov and Cheverda, 2005; 2006). However, it is more economical to launch beams from the source and receiver positions down into the subsurface since there are fewer source and receiver locations than subsurface scattering points, and this minimizes the amount of beam tracing required. In order to locate the beam-waists in the subsurface when the beams are launched from the source and receiver aperture, then generally curved beam fronts are required along the source and receiver aperture.

For dynamic beam focusing in Gaussian beam imaging, the beams are launched from the initial source and receiver plane, but then are dynamically-focused for each of the individual scattering points. Although the beams are generally non-planar along the receiver plane, the initial beam parameters can be determined from the specified beam parameters at depth. However, now these curved beams on the initial surface must be matched to the local slant stacks of the data for beam parameters specified at each of the sub-surface scattering points.

Assuming that the initial beam parameters have been determined from dynamic ray tracing for beam parameters specified at the scattering points, then the algorithm for imaging focused Gaussian beams from Nowack (2008) can be extended to dynamic focusing. For generally non-planar initial beams at the source or receiver locations launched at some angle to the aperture plane, the quadratic part of the initial beam with respect to the horizontal x coordinate can be written

$$\exp\left\{\frac{-\omega}{2}\frac{K_x(s_0)}{v_0}(x-x_L)^2\right\}\exp\left\{\frac{-(x-x_L)^2}{2L^2_{x-\mathrm{ref}}(s)}\right\} \tag{2.19}$$

where $K_x(s_0)$ is the initial horizontal beam curvature, and $L_{x-\mathrm{ref}}(s_0)$ is the initial horizontal beam half-width at the reference frequency ω_{ref}. To match this with the initial parameters of the beam propagated into the medium, then the transverse coordinate of the beam $n = \cos\gamma(x - x_L)$ where γ is the angle of the beam with respect to the vertical. Given the initial values $K_x(s_0)$ and $L_{x-\mathrm{ref}}(s_0)$ along the source and receiver aperture, then the initial values for $M_R(s_0)$ and $M_I(s_0)$ for the beams are

$$M_R(s_0) = \frac{K_x(s_0)}{v_0\cos^2(\gamma)} \tag{2.20}$$

and

$$M_I(s_0) = (\omega_{\mathrm{ref}}\cos^2(\gamma)L^2_{x-\mathrm{ref}}(s_0))^{-1} \tag{2.21}$$

and then the initial beam parameter $\varepsilon = \varepsilon_r - \mathrm{i}\varepsilon_i$ can be obtained and used to construct the beam solution propagated into the medium.

The 2-D resolution of unity by Gaussian functions in the aperture plane is

$$1 \sim \frac{1}{\sqrt{2\pi}}\frac{\Delta L}{\sigma}\sum_{m=-\infty}^{\infty}\mathrm{e}^{-(x-m\Delta L)^2/2\sigma^2} \tag{2.22}$$

where

$$\Delta L \ll 2\sigma\ . \tag{2.23}$$

Assuming a regularly spaced set of beam centers $x_L = m\Delta L$ along the receiver array, the initial locations of the Green's functions at the receivers can be phase shifted to these beam center locations with a phase adjustment of $p^g_1(x^g_1 - m\Delta L) + \frac{K_x(s_0)(x^g_1-m\Delta L)^2}{2v_0}$. Then,

$$g(\underline{x},\underline{x}^g,\omega) \sim C^g\int\frac{\mathrm{d}p^g_1}{p^g_3}u^{\mathrm{gb}}(\underline{x},\underline{x}^L,\underline{p}^g,\omega)\mathrm{e}^{\mathrm{i}\omega(p^g_1(x^g_1-m\Delta L)+\frac{K_x(s_0)(x^g_1-m\Delta L)^2}{2v_0})}\ , \tag{2.24}$$

where C^g is a coefficient for the receiver Green's functions and p^g_1 is the horizontal component of the ray parameter vector along the receiver aperture. The imaging formula can then be written

$$I_s(\underline{x}) = \sum_{m=-\infty}^{\infty}\int\frac{d\omega}{2\pi}A_1(\omega)\int d\underline{x}^g\int\frac{\mathrm{d}p^g_1}{p^g_3}\bar{u}^{\mathrm{gb}}(\underline{x},\underline{x}^L,\underline{p}^g,\omega)\mathrm{e}^{-\mathrm{i}\omega(p^g_1(x^g_1-m\Delta L)+\frac{K_x(s_0)(x^g_1-m\Delta L)^2}{2v_0})} \tag{2.25}$$
$$\bar{g}(\underline{x},\underline{x}^s,\omega)u_s(\underline{x}^r,\underline{x}^s,\omega)\mathrm{e}^{-(x^g_1-m\Delta L)^2/2\sigma^2}$$

where

$$A_1(\omega) = \left(\frac{+\mathrm{i}}{2\pi}\right)\left(\frac{\bar{\varepsilon}}{v_0^g}\right)^{1/2}\omega^2\bar{S}(\omega)\frac{1}{\sqrt{2\pi}}\frac{\Delta L}{\sigma}\ . \tag{2.26}$$

The source Green's function now needs to be decomposed into Gaussian beams, but for simplicity here will be just referred to as $\bar{g}(\underline{x},\underline{x}^s,\omega)$, where the over-bar signifies the complex conjugate.

The common-shot imaging formula for non-planar, focused beams along the aperture plane can then be written

$$I_s(\underline{x}) = \sum_{m=-\infty}^{\infty}\int\frac{d\omega}{2\pi}\int\frac{\mathrm{dp}_1^g}{p_3^g}A_1(\omega)\bar{g}(\underline{x},\underline{x}^s,\omega)\bar{u}^{\mathrm{gb}}(\underline{x},\underline{x}^L,\underline{p}^g,\omega)D_p(\underline{x}^L,\underline{x}^s,\underline{p}^g,\omega) \tag{2.27}$$

where

$$D_p(\underline{x}^L,\underline{x}^s,\underline{p}^g,\omega) = \int \mathrm{dx}_1^g u_s(\underline{x}^g,\underline{x}^s,\omega)\mathrm{e}^{-(x_1^g-m\Delta L)^2/2\sigma^2}\mathrm{e}^{-\mathrm{i}\omega(p_1^g(x_1^g-m\Delta L)+\frac{K_x(s_0)(x_1^g-m\Delta L)^2}{2v_0})} \tag{2.28}$$

This is a local slant-stack of the data with a quadratic phase correction term to match the data with the beams launched into the medium. The standard Gaussian beam migration formulas with the planar beam waists along the aperture plane does not include this quadratic phase correction term (Hill, 1990; 2001; Hale, 1992; Nowack et al., 2003). The beam centers are spaced along the receiver aperture plane at

$$x_1^L = m\Delta L, \qquad \Delta L \ll 2\sigma\ . \tag{2.29}$$

and the initial horizontal beam widths are

$$\sigma = L_{x-\mathrm{ref}}(s_0)\left(\frac{\omega_r}{\omega}\right)^{1/2} \tag{2.30}$$

where $L_{x-\mathrm{ref}}(s_0)$ is the horizontal half-width of an initial Gaussian function at the reference frequency ω_{ref}. The spacing of the beams in horizontal position and launch angle can then be determined based either on physical reasoning (Hill, 1990; 2001; Hale, 1992; Nowack et al., 2003), or by arguments based on frames (Feichtinger and Strohmer, 1998). However, for curved beams along the initial plane, the data windows need to be broader to account for the wider beams at the surface.

3. Applications of Dynamically-Focused Gaussian beam Migration. In order to test the dynamically-focused beam migration formulation, two examples are given. The first application has 5 compact sources located at depths of 8,000, 12,000, 16,000, 20,000 and 24,000 ft at a distance of 40,000 ft from the left side of the model. The background velocity model has two layers. The first layer has a thickness of 6000 ft with a constant velocity of 5000 ft/sec. The second layer goes from 6000 ft to 30,000 ft in depth with a vertical velocity gradient of $v(z) = v_0 + k(z - z_b)$ where $v_0 = 5000$ ft/sec, and $k = .15$. The shot position is located along the surface at a horizontal position of 40,000 ft from the left side of the model. The receiver array is from 25,000 ft to 55,000 ft on the surface. Figure 1 shows the computed wavefield from the 5 compact scatterers. The sampling rate is .008 sec and the peak frequency of the data is 5 Hz.

Figure 2 shows the partial image of the data from a single vertically propagated Gaussian beam with the planar wavefront at the surface. For simplicity the source side Green's function is constructed separately using Gaussian beams that are planar at the source location for all the

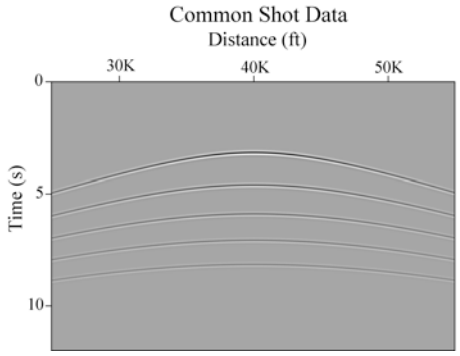

FIG. 1. *Computed common-shot data is shown for a shot point on the surface at a position of 40,000 ft. The receiver array is from 25,000 ft to 55,000 ft. Diffractions from 5 compact scatterers are shown each with a horizontal position of 40,000 ft and depths of 8,000, 12,000, 16,000, 20,000 and 24,000 ft.*

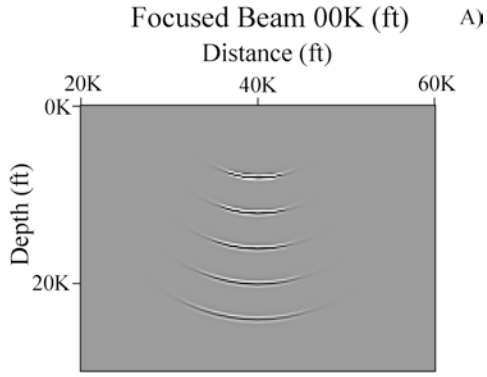

FIG. 2. *The partial image of the common shot data in Figure 1 using a single vertical Gaussian beam at a receiver position at 40,000 ft using a beam with a planar beam-waist at the surface.*

examples given. Note on the figure that the images of the diffractors are curved and increase in width with depth. Figure 3 shows the partial image of the common shot data in Figure 1 using a single vertical Gaussian beam at a receiver position at 40,000 ft using a focused beam with the beam-waist at a depth of 12,000 ft. Now the diffractor at a depth of 12,000 ft is the most focused using a single beam with the images of the other diffractors being broader and generally curved.

Figure 4 shows the partial image of the common shot data in Figure 1 using a single vertical Gaussian beam at a receiver position at 40,000 ft using dynamic focusing with the beam waist now specified at all depths. Now the partial image of the scatterers all have similar images with plane beam waists of the same beam widths for all scatterers. It would look as if we had been able to perform Gaussian beam migration with non-diffracting Gaussian beams. However, actually the image is formed with a number of different Gaussian beams for all scattering points in the medium such that in a dynamic fashion the beams have the same planar beam waists and beam widths at each scatterer.

Figure 5 shows the complete dynamically-focused Gaussian beam image for the single shot gather from Figure 1 using beams from all beam center locations launched at a range of angles. This results in focused images of all 5 scatterers and indicates that the imaging is being properly applied even with the shifted beam-waists of the individual beam components for all imaging points of the medium. The small tails result from the limited angle range for the summation of the beams.

The dynamically-focusing beam approach is now applied to a single shot gather from the Sigsbee2A data set distributed by SMAART (Subsalt Multiples Attenuation and Reduction Team) and

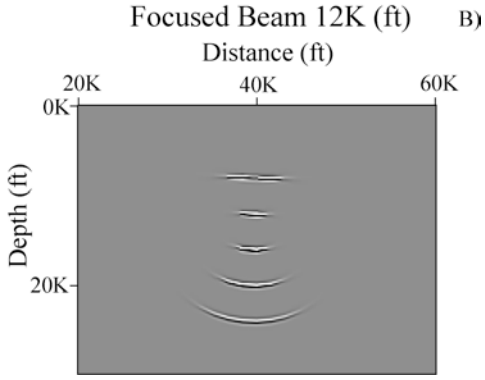

FIG. 3. *The partial image of the common shot data in Figure 1 using a single vertical Gaussian beam at a receiver position at 40,000 ft using a focused beam with a beam-waist at a depth of about 12,000 ft.*

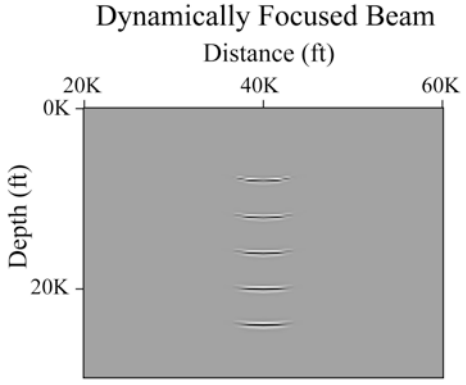

FIG. 4. *The partial image of the common shot data in Figure 1 using a vertical dynamically-focused beam.*

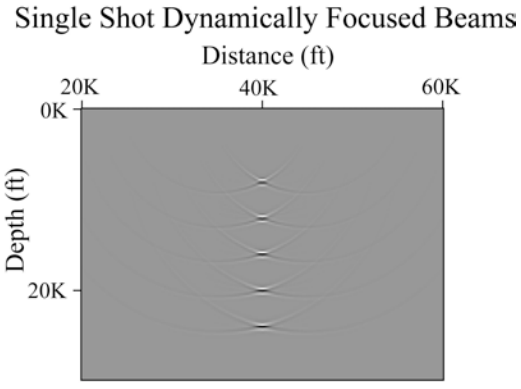

FIG. 5. *The Gaussian beam image is shown using the single shot gather in Figure 1 with beams from all beam positions launched at a range of angles, each with dynamically-focused beams. This results in focused images of all 5 scatterers and indicates that the imaging is being properly applied even with dynamically-focused individual beam components.*

available at http://www.delphi.tudelft.nl/SMAART/. In order to test the focused beam approach, a single shot gather with a shot location at 6,325 ft from the left edge of the model is used. The

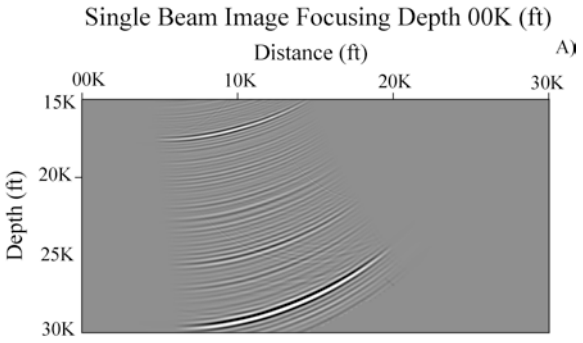

FIG. 6. *This shows the partial imaging result for a single Gaussian beam with the beam-waist at the surface along the receiver array for a single shot gather from the Sigsbee2A dataset.*

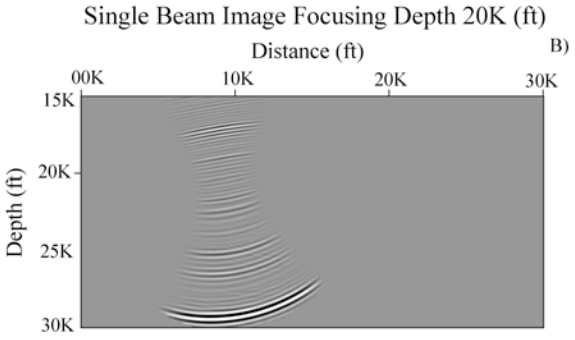

FIG. 7. *This shows the partial imaging result for a single Gaussian beam with the beam-waist shifted to about 20,000 ft in depth for a single shot gather from the Sigsbee2A dataset.*

receiver array starts at the shot location and has a maximum offset of 26,025 ft with a spacing of 75 ft. The background velocity model has the first layer from the surface down to the seafloor with a velocity of 5000 ft/sec. The second layer goes from seafloor to 30,000 ft in depth with a background velocity of $v(z) = v_0 + k(z - z_{\text{seafloor}})$ where $v_0 = 5000$ ft/sec, and $k = .30$. A salt dome exists with a velocity of *14,800 ft/sec* in the middle and right parts of the model, but for the tests here only a shot gather away from the salt dome is used.

In Figure 6, the partial imaging for a single Gaussian beam is shown with the planar beam-waist at the surface receiver depth. As in the earlier examples the source side Green's function is constructed separately using Gaussian beams that are planar at the source location. The receiver Gaussian beam has an initial location near the source and the partial image for a beam with a slight angle from the vertical is shown. As in the earlier example, when the beam-waist is at the surface receiver depth, then curved beam fronts result which broaden with depth over the depth range of the model shown between 15,000 and 30,000 ft. This is typical of standard implementations of Gaussian beam migration. However, in regions of a complicated background medium, the medium itself can cause additional focusing of the beams.

Figure 7 shows the partial imaging results for a single Gaussian beam with the beam-waist shifted to about 20,000 ft in depth. At this depth, the narrowest part of the beam image occurs. If the target structure were located at this depth, then fewer beams would be required to form a complete image. Also, the beam images would have planar beam fronts at this depth leading to more stable images. However, as shown in Figure 7 at other depths the partial image results in curved and broader beam fronts.

Figure 8 shows the imaging results using dynamic focusing where all sub-surface points have

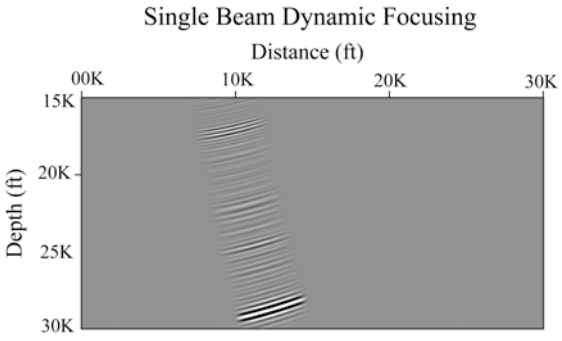

FIG. 8. *This shows the partial imaging result for a single dynamically-focused beam from the Sigsbee2A dataset.*

planar beams with the same beam width. This has the appearance of an image from a single non-diffracting beam, but since Gaussian beams generally diffract, this is really a composite image for Gaussian beams with multiple imaging depths for a single central beam. This type of imaging is important with certain true amplitude formulations where planar and localized beams are required at the imaging points in the sub-surface (Protosov and Cheverda, 2005, 2006). But, these formulations originally involved launching beams directly from the scattering points in the sub-surface up to the surface. In the faster alternative proposed here, dynamically-focused Gaussian beams are launched from the surface down to the imaging points at depth instead. Nonetheless, the use of dynamically-focused Gaussian beams is still slower than traditional Gaussian beam imaging or imaging using focused Gaussian beams with a single focusing depth. However, pre-computing dynamically-focused slant stacks of the data can be implemented to improve the speed of the algorithm and needs to be further explored in future work.

4. Conclusions. The application of dynamically-focused Gaussian beams has been initially investigated for seismic imaging and is an extension of the focused beam approach of Nowack (2008). The shifting of the beam-waists away from the source and receiver aperture adds flexibility to Gaussian beam algorithms allowing for the narrowest portions of the beams to occur at the depth of a specific target structure. This minimizes the number of beams required to form an image at the target depth. Also, at the beam-waists the beam fronts are planar leading to more stable beam summations for imaging. To match with the surface data, quadratic phase corrections are required for the local slant-stacks of the data. Using dynamically-focused Gaussian beams allows for beams to have planar wavefronts and the same beam widths at all scattering points in the sub-surface. It has the appearance of using non-diffracting Gaussian beams, but since all Gaussian beams diffract, this is really the result of using beams with multiple focusing depths. The use of planar and localized Gaussian beams at all the sub-surface scattering points also has advantages with regard to certain true amplitude imaging formulations. However, using dynamically-focused Gaussian beams from the surface down to the scattering points avoids having to launch beams from every scattering point in the medium up to the surface. Nonetheless, dynamically-focused Gaussian beam imaging is still slower than using either traditional Gaussian beam imaging or using a single focusing depth for imaging. Dynamically-focused imaging was initially tested using a single shot gather for a model with 5 scatterers at different depths, and then for a dynamically-focused Gaussian beam from the Sigsbee2A model.

Acknowledgments. This work was supported in part by the National Science Foundation and the Air Force Geophysics Laboratory and partly by the members of the Geo-Mathematical Imaging Group (GMIG) at Purdue University.

REFERENCES

[1] Babich, V.M and M.M. Popov (1989) *Gaussian summation method (Review)*, Izvestiya Vysshikh Uchebnykh Zavedenii, Radiofizika 32, 1447-1466 (Translated in Radiophysics and Quantum Electronics 32, 1063-1081, 1990).

[2] Bleistein, N. (2007) *Mathematics of modeling, migration and inversion with Gaussian beams*, Lecture Notes (online at http://www.cwp.mines.edu/~norm/).

[3] Cerveny, V. (1985a) *Gaussian beam synthetic seismograms*, J. Geophys., 58, 44-72.

[4] Cerveny, V. (1985b) *The applications of ray tracing to the numerical modeling of seismic wave fields in complex structures*, in Seismic Shear Waves (ed. G. Dohr) Geophysical Press, London, pp. 1-124.

[5] Cerveny, V. (2000) *Seismic Ray Theory*, Cambridge University Press.

[6] Cerveny, V., L. Klimes and I. Psencík (2007) *Seismic ray method: some recent developments*, Advances in Geophysics, 48, 1-128.

[7] Cerveny, V., M.M. Popov and I. Psencík (1982) *Computation of wavefields in inhomogeneous media – Gaussian beam approach*, Geophys. J.R. Astr. Soc., 70, 109-128.

[8] Feichtinger, H.G. and T. Strohmer (Eds.) (1998) *Gabor Analysis and Algorithms: Theory and Applications*, Birkhauser.

[9] Hale, D. (1992) *Migration by the Kirchhoff, slant stack and Gaussian beam methods*, CWD-121, Center for Wave Phenomena, Colorado School of Mines, Golden, CO.

[10] Hill, N. R. (1990) *Gaussian beam migration*, Geophysics, 55, 1416-1428.

[11] Hill, N. R. (2001) *Prestack Gaussian beam depth migration*, Geophysics, 66, 1240-1250.

[12] Lugara, D., C. Letrou A, Shlivinski, E. Heyman and A. Boag (2003) *Frame-based Gaussian beam summation method: Theory and applications*, Radio Science, Vol. 38, No. 2, 8026.

[13] Nowack, R.L. (2003) *Calculation of synthetic seismograms with Gaussian Beams*, Pure and Applied Geophys., 160, 487-507.

[14] Nowack, R.L. and K. Aki (1984) *The two-dimensional Gaussian beam synthetic method: testing and application*, J. Geophys. Res., 89, 7797-7819.

[15] Nowack, R.L., M.K. Sen, and P.L. Stoffa (2003) *Gaussian beam migration of sparse common-shot data*, SEG Expanded Abstracts, Seventy-Third Annual Meeting, Society of Exploration Geophysicists, Tulsa, pp. 1114-1117.

[16] Popov, M. M. (1982) *A new method of computation of wave fields using Gaussian beams*, Wave Motion, 4, 85-97.

[17] Popov, M. M. (2002) *Ray Theory and Gaussian beam method for geophysicists*, Lecture notes University of Bahia, Salavdor Brazil, 172 pp.

[18] Protasov, M.I. and V.A. Cheverda (2005) *True amplitude Gaussian beam imaging*, Proceedings of the International Seminar "Days on Diffraction – 2005", June 28-July 1 2005, St. Petersburg, Russia, pp. 225-234.

[19] Protasov, M.I. and V.A. Cheverda (2006) *True-amplitude seismic imaging*, Doklady Earth Sciences, Vol. 407A, 441-445.